

Self-supervised Learning of Latent Space Dynamics

YUE LI, ETH Zürich, Switzerland

GENE WEI-CHIN LIN, Meta Reality Labs, Canada

EGOR LARIONOV, Meta Reality Labs, USA

ALJAŽ BOŽIĆ, Meta Reality Labs, Switzerland

DOUG ROBLE, Meta Reality Labs, USA

LADISLAV KAVAN, Meta Reality Labs, Switzerland

STELIAN COROS, ETH Zürich, Switzerland

BERNHARD THOMASZEWSKI, ETH Zürich, Switzerland

TUUR STUYCK, Meta Reality Labs, USA

HSIAO-YU CHEN, Meta Reality Labs, USA

Modeling the dynamic behavior of deformable objects is crucial for creating realistic digital worlds. While conventional simulations produce high-quality motions, their computational costs are often prohibitive. Subspace simulation techniques address this challenge by restricting deformations to a lower-dimensional space, improving performance while maintaining visually compelling results. However, even subspace methods struggle to meet the stringent performance demands of portable devices such as virtual reality headsets and mobile platforms. To overcome this limitation, we introduce a novel subspace simulation framework powered by a neural latent-space integrator. Our approach leverages self-supervised learning to enhance inference stability and generalization. By operating entirely within latent space, our method eliminates the need for full-space computations, resulting in a highly efficient method well-suited for deployment on portable devices. We demonstrate the effectiveness of our approach on challenging examples involving rods, shells, and solids, showcasing its versatility and potential for widespread adoption.

CCS Concepts: • **Computing methodologies** → **Physical simulation**.

Additional Key Words and Phrases: Subspace Simulation, Autoencoder, Latent Space Integration, Self-supervised Learning

ACM Reference Format:

Yue Li, Gene Wei-Chin Lin, Egor Larionov, Aljaž Božić, Doug Roble, Ladislav Kavan, Stelian Coros, Bernhard Thomaszewski, Tuur Stuyck, and Hsiao-yu Chen. 2025. Self-supervised Learning of Latent Space Dynamics. *Proc. ACM Comput. Graph. Interact. Tech.* 8, 4, Article 57 (August 2025), 18 pages. <https://doi.org/10.1145/3747854>

1 INTRODUCTION

Modeling the dynamic behavior of elastic objects is essential for creating realistic virtual environments. Physics-based simulations can produce highly compelling results, capturing the complex

Authors' addresses: Yue Li, ETH Zürich, Switzerland, yue.li@inf.ethz.ch; Gene Wei-Chin Lin, Meta Reality Labs, Canada, genelin@meta.com; Egor Larionov, Meta Reality Labs, USA, elrmv@meta.com; Aljaž Božić, Meta Reality Labs, Switzerland, aljazz@meta.com; Doug Roble, Meta Reality Labs, USA, droble@meta.com; Ladislav Kavan, Meta Reality Labs, Switzerland, lkavan@meta.com; Stelian Coros, ETH Zürich, Switzerland, stelian.coros@inf.ethz.ch; Bernhard Thomaszewski, ETH Zürich, Switzerland, bthomasz@ethz.ch; Tuur Stuyck, Meta Reality Labs, USA, tuur@meta.com; Hsiao-yu Chen, Meta Reality Labs, USA, hsiaoyu@meta.com.

Permission to make digital or hard copies of all or part of this work for personal or classroom use is granted without fee provided that copies are not made or distributed for profit or commercial advantage and that copies bear this notice and the full citation on the first page. Copyrights for components of this work owned by others than ACM must be honored. Abstracting with credit is permitted. To copy otherwise, or republish, to post on servers or to redistribute to lists, requires prior specific permission and/or a fee. Request permissions from permissions@acm.org.

© 2025 Association for Computing Machinery.

2577-6193/2025/8-ART57

<https://doi.org/10.1145/3747854>

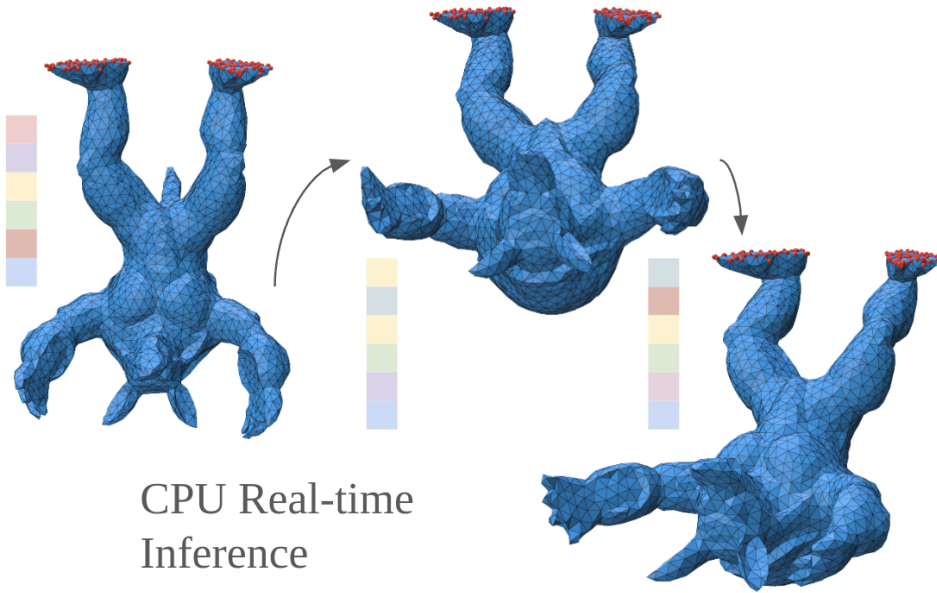


Fig. 1. **Real-time Simulation:** We propose a novel latent space integrator that allows for robust and stable CPU-real-time (0.489 ms per frame) autoregressive inference of dynamic motions. Boundary conditions are shown as red spheres and the colored squares indicate low-dimensional latents.

dynamics induced by interactions between digital humans and virtual objects. However, these simulations are computationally expensive, and even the most advanced methods struggle to meet the stringent real-time requirements of computer games, telepresence, or virtual reality applications.

Subspace simulation methods offer a promising alternative, providing an efficient trade-off between speed and generality. By focusing on the most likely object deformations, subspace approaches can accelerate simulations by orders of magnitude. However, most methods still require frequent evaluations of full-space energies and their derivatives during time stepping. These full-space evaluations require significant computational resources, precluding their deployment on compute-limited devices. As a result, achieving true real-time performance remains elusive even with subspace simulation methods. In this work, we present a novel approach for neural simulation of deformable objects with natural dynamics. Unlike previous work, our method operates entirely in latent space, removing the need to evaluate full-space energies and their derivatives. Our two-step process begins with training an autoencoder on data sequences, followed by training a multilayer perceptron to predict an implicit integration step using initial positions and velocities in latent space. We build our method on a self-supervised learning approach that uses the variational implicit Euler potential as a loss function. We demonstrate that this self-supervised approach significantly improves generalization when compared to conventional supervised methods. To ensure stable autoregressive inference, we propose a novel data augmentation strategy that adds noise to single-step predictions during training. This approach leads to improved stability for long roll-outs while avoiding multi-step predictions during training. We further identify a data imbalance issue that arises from physics-based self-supervised learning and propose a simple yet effective normalization strategy.

We evaluate our method on a diverse set of examples that involve dynamic motions of elastic rods, shells, and solids. The results demonstrate that our latent-space integrator produces stable and plausible animations at a fraction of the computational cost required by full-space simulations. In summary, our contributions are

- a novel method for implicit integration of elastodynamics equations in latent space using self-supervised learning.
- a subspace simulation method that operates exclusively in latent space during inference.
- a dedicated data augmentation and balancing method for improved stability and generalization.

2 RELATED WORK

Subspace Simulation in Graphics. Subspace simulation techniques have been extensively explored in the field of computer graphics to efficiently model complex dynamic systems [Sharp et al. 2023; Sifakis and Barbic 2012a], e.g. shells [Zheng et al. 2024], cloths [De Aguiar et al. 2010; Hahn et al. 2014; Holden et al. 2019; Li et al. 2023], deformable bodies [Barbič and James 2005; Chen et al. 2023; Harmon and Zorin 2013; Wang et al. 2015; Wu et al. 2015; Zheng and Barbic 2024], animated characters [Barbič et al. 2009, 2012; Jacobson et al. 2012] and fluids [Kim and Delaney 2013; Treuille et al. 2006]. A common strategy is to construct subspace bases from the elastic energy Hessian at the rest state. Early works focus on linear modal analysis [Hauser et al. 2003; Pentland and Williams 1989; Sifakis and Barbic 2012b] several extension to the nonlinear setting have recently been proposed [Benckroun et al. 2023; Duenser et al. 2022; Wang et al. 2024].

While the eigenvectors of the elastic energy Hessian might be informative enough to construct reduced bases for deformable solids, hair exhibits a much less structured behavior. Arguably the most widely used approach for hair simulation is based on *guided strands* [Chai et al. 2014; Hsu et al. 2024; Lyu et al. 2020], which involves simulating a select group of guide hairs from which the remaining hairs are interpolated. Hair meshes [Wu and Yuksel 2016; Yuksel et al. 2009] are an alternative approach which also allows for real-time rendering [Bhokare et al. 2024]. However, this approach requires (often manually) precomputed hair meshes with fixed topologies. Furthermore, this method is not appropriate for low-end devices as it requires dedicated GPU resources with mesh shader functionality, which is often absent from mobile hardware. To accommodate different types of deformable objects, we construct the map from reduced space to full space using deep neural networks, namely autoencoders.

Physics-informed Learning. There has been an ongoing trend of leveraging physics-based loss functions to ground data-driven methods in computer vision and graphics [Bertiche et al. 2020, 2022; Chentanez et al. 2020; Li et al. 2021; Modi et al. 2024; Santesteban et al. 2022]. Early work performs physics-based simulation on the fly to either generate physics-based targets as supervisions [Li et al. 2021] or correct self-intersections during reconstruction [Halimi et al. 2022]. Recent endeavors aim to learn the time integration function directly. In the supervised setting, Pfaff et al. [2020] and Sanchez-Gonzalez et al. [2020] employ graph neural networks to simulate particles and meshes. Similar to our work that adopts a self-supervised learning strategy, Bertiche et al. [2020; 2022], Santesteban et al. [2022], and Grigorev et al. [2024; 2023] learn quasi-static and dynamic integrators for cloth driven by articulated characters. Most recently, Stuyck et al. [2025] propose a self-supervised strategy for learning hair quasi-statics. Whereas previous work focuses on learning full-space integrators, our method is the first to apply the self-supervised training paradigm in learning subspace integrators. We demonstrate that the resulting network is extremely lightweight and leads to real-time CPU performance.

Reduced Modeling with Neural Networks. There has been a recent surge in using deep neural networks as smooth and compact representations for reduced modeling. Zong *et al.* [2023] leverage neural networks as implicit reduced representations for stress fields and Chen *et al.* [2023] model the deformation map for material point methods using neural representations. Utilizing deep neural networks directly on position levels for model reduction but working with continuous fields, Chen *et al.* [2022] and Chang *et al.* [2023] learn smooth deformation maps from undeformed fields to deformed ones. Pan *et al.* [2023] further leverage implicit representations for spatial-temporal data. In a similar vein but closely related to our work, Lee and Carlberg [2020], Fulton *et al.* [2019], Zhang *et al.* [2021] and Shen *et al.* [2021] use autoencoders to condense high dimensional position vectors into a low dimensional latent space. Additionally one could further improve the convergence by enforcing Lipschitz continuity [Lyu et al. 2024]. Similar in that we also resort to the autoencoder to construct a reduced subspace, we demonstrate that a physics-based integrator can be learned directly in this latent space.

3 METHOD

Our approach learns a time integration scheme in a nonlinear latent space (see Fig. 2). To construct the latent space, we begin by generating full-space motion data using an off-the-shelf simulation method (Sec. 3.1). We then construct a low-dimensional nonlinear subspace from these data using autoencoders (Sec 3.2). At the core of our approach, we learn an integrator in the subspace in a self-supervised manner by minimizing the full-space incremental potential (Sec 3.3).

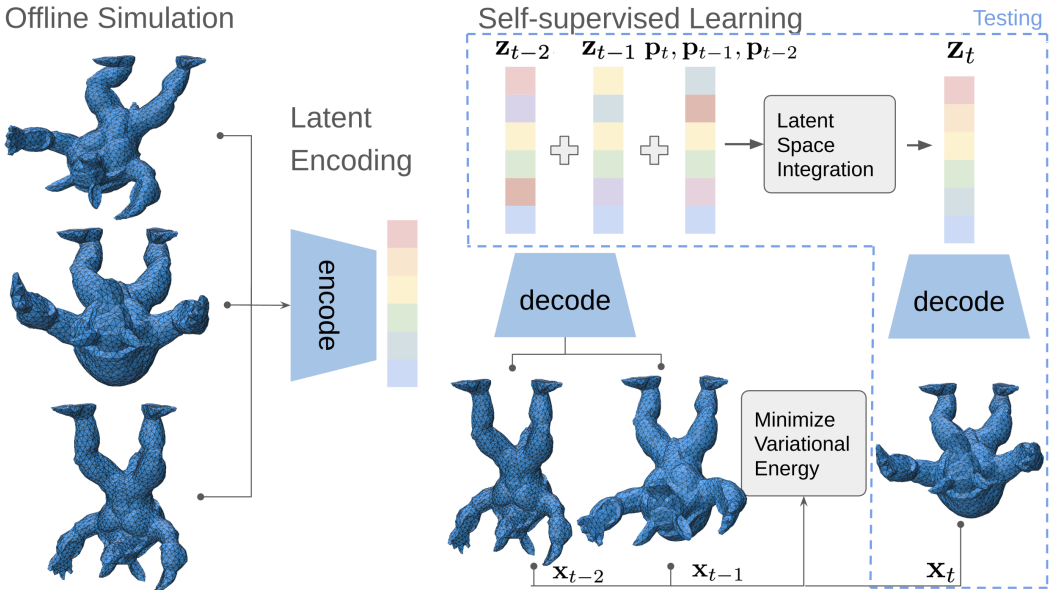


Fig. 2. **Method Overview:** Our approach encodes full-space simulation data into low-dimensional latent vectors. We then learn an integrator in latent space in a self-supervised setting by minimizing the incremental potential in full space. During testing, as indicated by the blue dashed region, our integrator does not require any full-space computation and therefore runs in real-time on CPU.

3.1 Full Space Simulation

We initiate our approach by defining the full space energy that describes the physical system. This energy serves two key purposes: it generates the training data and supervises the training of the subspace integrator.

To enable robust simulation, we employ implicit Euler as our time-stepping strategy. Following [Martin et al. 2011], we cast the nonlinear root-finding problem into an optimization problem. At each simulation time step, we find the end-of-time-step position \mathbf{x}_t by minimizing the objective function

$$E_{\text{total}} = E_{\text{inertial}}(\mathbf{x}_t, \mathbf{x}_{t-1}, \mathbf{x}_{t-2}) + E_{\text{elastic}}(\mathbf{x}_t, \mathbf{X}) + E_{\text{external}}(\mathbf{x}_t), \quad (1)$$

where \mathbf{X} denotes the rest state positions. These energies follow standard practices in graphics, E_{inertial} computes the inertial energy given three consecutive positions, E_{external} computes the energy due to external forces. The elastic potential E_{elastic} differs across applications. For rods, we use the stretching and bending models from Bergou et al. [2008]. We use discrete elastic shells [Grinspun et al. 2003] to model the material behavior of cloth, and linear tetrahedral elements with the StVK energy [Sifakis and Barbic 2012b] for solids.

We minimize this objective energy using Newton's method with backtracking line search [Nocedal and Wright 1999]. To ensure robust convergence, we project local Hessian blocks to be positive-definite [Teran et al. 2005]. Boundary conditions are imposed by removing the corresponding degrees of freedom from the system and setting the displacements to prescribed values.

3.2 Latent Space Representation

We utilize autoencoder as a convenient tool to compress full-space simulation data to an efficient nonlinear low-dimensional subspace. We learn this nonlinear map by minimizing the reconstruction loss in full space

$$\min_{\theta_d, \theta_e} \sum_t \|\mathcal{D}(\mathcal{E}(\mathbf{x}_t; \theta_e); \theta_d) - \mathbf{x}_t\|_2^2, \quad (2)$$

where θ_e and θ_d are the network parameters for the encoder \mathcal{E} and decoder \mathcal{D} . We further refer to the output of the bottleneck layer $\mathbf{z}_t := \mathcal{E}(\mathbf{x}_t; \theta_e)$ as latents. To remove high-frequency artifacts in the reconstruction, we initialize the first layer of the encoder and the last layer of the decoder with PCA bases following Fulton et al. [2019]. We encode vertex positions relative to Dirichlet boundary conditions. For rods, we leverage root relative encodings, *i.e.*, every vertex along a given rod is coded by the relative distances to the root. We exclude root vertices from the latents and simply apply the boundary condition values whenever decoded to full states. For our cloth and solid examples, we encode the mesh vertices relative to the mean position of the Dirichlet vertices.

3.3 Latent Space Self-supervised Learning

To achieve real-time performance, we learn an integrator \mathcal{I} that does not require any evaluation in full space during inference. Similar to a first-order numerical integrator in full space, our integrator also takes the previous two states (latents) and the boundary condition history as inputs and predicts the corresponding latent codes for the current frame,

$$\mathbf{z}_t = \mathcal{I}(\mathbf{z}_{t-1}, \mathbf{z}_{t-2}, \mathbf{p}_t, \mathbf{p}_{t-1}, \mathbf{p}_{t-2}; \theta_{\mathcal{I}}), \quad (3)$$

where $\theta_{\mathcal{I}}$ denotes the weights and biases of the integrator network and the parameters $\mathbf{p}_t, \mathbf{p}_{t-1}, \mathbf{p}_{t-2}$ are boundary conditions for three consecutive steps. For instance, for the rod swing example in

Fig. 3, these are the three-time-step velocities of the moving cube. Our integrator predicts new frames directly with a time step $\Delta t = 1/30$ seconds per frame.

Given that we have ground truth latents available, one alternative is to adopt a supervised learning strategy to penalize the mismatch between the network prediction and the ground truth data in the L_2 sense. This approach, albeit simple, is inclined to overfitting and often fails to generalize [Ma et al. 2023; Zehnder et al. 2021]; see also Fig. 8.

Inspired by recent advances in physics-informed learning, we propose a novel self-supervised learning strategy. While there isn't a closed-form functional defined in latent space, we can decode the latents to their full space configurations and then minimize the variational implicit Euler loss. Therefore, the loss function we used for learning the integrator is identical to the objective function that we minimize during full space simulation, except that now the optimization variables are neural network weights and biases, θ_I , instead of positions. Denoting the inputs of the latent integrator as \mathbf{q} , our loss function reads

$$\begin{aligned} \mathcal{L}(\theta_I) = & E_{\text{inertial}}(\mathbf{x}_t(\mathbf{z}_t(\mathbf{q}; \theta_I)), \mathbf{x}_{t-1}, \mathbf{x}_{t-2}) \\ & + E_{\text{external}}(\mathbf{x}_t(\mathbf{z}_t(\mathbf{q}; \theta_I))) + E_{\text{bc}}(\mathbf{x}_t(\mathbf{z}_t(\mathbf{q}; \theta_I))) \\ & + E_{\text{elastic}}(\mathbf{x}_t(\mathbf{z}_t(\mathbf{q}; \theta_I)), \mathbf{X}) . \end{aligned} \quad (4)$$

As demonstrated by the results, our physics-based loss function significantly improves the generalization ability of the trained network. For rod examples, we exclude the boundary condition term as it is enforced as hard constraints. For cloth and solid examples, we use a quadratic penalty potential, $E_{\text{bc}}(\mathbf{x}_t) = w_{\text{bc}} \|\mathbf{x}_t - \mathbf{x}_t^*\|_2^2$, to enforce boundary conditions, where \mathbf{x}_t^* is the target position at time step t .

Data Augmentation. During training, we use ground truth latents from training data and predict latents only for one step. This by itself cannot guarantee stability during auto-regressive inference. While one alternative is to predict multiple steps during training [Grigorev et al. 2023], the complexity of the training graph can increase significantly.

We propose a simpler alternative without the need to predict longer time horizons during training. Inspired by works on learning integrators in full space [Pfaff et al. 2020; Sanchez-Gonzalez et al. 2020], we augment our training data with the same amount of perturbed data. Specifically, for each batch, we add random noise sampled from a uniform distribution to the previous two latents scaled by 10% of the standard deviation of that batch while keeping the boundary conditions unchanged. Concretely, the integrator network also predicts $\tilde{\mathbf{z}}_t$ given the perturbed inputs $\tilde{\mathbf{z}}_{t-1}$ and $\tilde{\mathbf{z}}_{t-2}$

$$\tilde{\mathbf{z}}_t = \mathcal{I}(\tilde{\mathbf{z}}_{t-1}, \tilde{\mathbf{z}}_{t-2}, \mathbf{p}_t, \mathbf{p}_{t-1}, \mathbf{p}_{t-2}; \theta_I) . \quad (5)$$

The same loss function (Eqn. 4) is applied to $\tilde{\mathbf{z}}_t$. This training noise allows for efficient sampling of states that are not at dynamic equilibrium, and we are able to achieve this without additional data generation, thanks to our self-supervised setup. This enables stable autoregressive inference for thousands of frames.

Data Balancing. We observe that different systems can have significantly varying energy levels, which impact their optimization. In particular, the higher energy state tends to dominate the gradient, causing errors in the lower energy systems. To illustrate this, consider how changes in boundary conditions affect a system's total energy. Small changes might only slightly increase the energy, but larger changes can cause significant jumps in the inertial and elastic potential. To mitigate this data imbalance, we employ a normalization strategy. Specifically, we normalize the energies within batches using the averaged velocity derived from the full space positions of the latents of the previous two steps. This approach helps stabilize the optimization process and ensures more accurate results in diverse energy states.

The normalized loss per data point $\bar{\mathcal{L}}_i$ is then

$$\bar{\mathcal{L}}^i = \frac{\mathcal{L}^i}{|\mathbf{v}_{t-1}|}, \quad (6)$$

where $\mathbf{v}_{t-1} = \frac{1}{N} \sum_j^N \frac{\mathbf{x}_{t-1}^j - \mathbf{x}_{t-2}^j}{\Delta t}$ and N is the total number of vertices in full space.

Hyperparameters & Implementation Details. Due to the physical nature of our supervision, we do not need to balance our loss terms, which reduces the need for hyperparameter tuning. We use 10^5 as our penalty weights w_{bc} for enforcing Dirichlet boundary conditions for all examples. The parameters in the physics-based loss terms correspond to the real-world parameters of the simulated objects. For hair, we assume a density of 1.32g/cm^3 , and a radius of 0.7mm . We use 4×10^7 GPa as Young's modulus and compute the stretching and bending parameters based on Bergou *et al.* [2010]. For cloth, we use a Young's Modulus of 10^6 GPa and a Poisson ratio of 0.45 . We assume the cloth has a thickness of 0.3 cm and a density of 1.5×10^3 kg/m^3 . Finally, for our deformable solids, we use a Young's Modulus of 10^7 GPa, a Poisson ratio of 0.48 , and assume unit mass density.

Our full space simulation framework is adapted from an open-source C++ simulation framework [Li *et al.* 2024]. We implement the autoencoder and integrator training in PyTorch [Imambi *et al.* 2021]. Our autoencoder uses multilayer perceptron (MLP) based ResNet [He *et al.* 2016] with batch normalization and Swish activation functions. The encoder and decoder are symmetric in layers and number of neurons. Our neural integrator also leverages an MLP-based network with Swish activation functions. The exact network architecture can be seen in Table 2. For training both the autoencoder and the neural integrator we use a learning rate of 10^{-4} . We train our autoencoders for 20,000 epochs using a batch size of 500.

4 RESULTS

In this section, we demonstrate the versatility of our approach by showcasing its applicability to various domains, including discrete elastic rods, discrete elastic shells, and volumetric finite elements. Our method is capable of simulating highly nonlinear elastic deformations in real-time on a CPU with plausible dynamics. Furthermore, we emphasize the importance of two key components in our method: training noise and data balancing, both of which play crucial roles in ensuring stability and generating plausible simulation outcomes.

4.1 Rod Simulation

In the first two sets of experiments, we show that our approach enables real-time simulation for discrete elastic rods. We begin by anchoring the rods at their root vertices and then applying a horizontal translation in the image plane (see Fig. 3). During training, we generate a sequence of examples with different but constant velocities. The rods are moved in opposite directions at 10-frame intervals for a total of 100 frames. Our training data consists of 12 different sequences with boundary conditions moving at velocities ranging from 10 m/s to 120 m/s with increments of 10 m/s. At test time, we start with a fast and out-of-distribution velocity and suddenly decrease it by an order of magnitude. As can be seen from this sequence, our networks smoothly adapt to these changes in boundary conditions.

In the second example, we rotate the same group of rods under different angular velocities. We create the training set by rotating the group of rods using different but constant velocities. We first test the resulting network using both interpolated velocities in between training data points (first and second rows) and outside of the training distribution (last row). Our training data consists of seven simulation sequences, each containing 100 frames. At each sequence, we vary the angular

velocities from $0.1 \text{ }^\circ/\text{s}$ to $0.4 \text{ }^\circ/\text{s}$ in increments of $0.05 \text{ }^\circ/\text{s}$. As can be seen from Fig. 4, our method is able to adapt to these changes and produces plausible and stable dynamics.

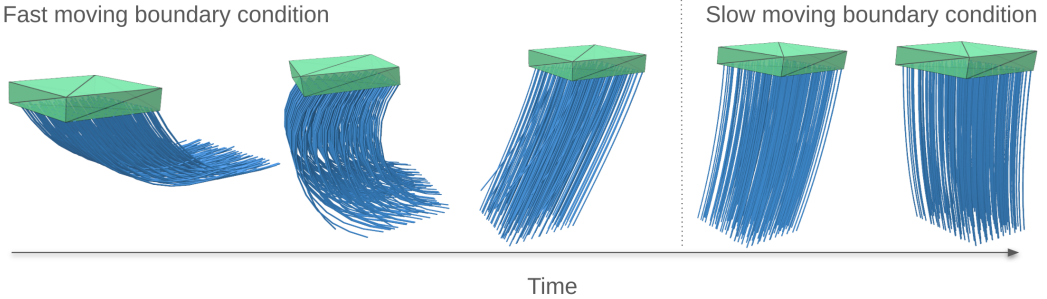


Fig. 3. **Accelerating and Decelerating Rods:** Thanks to our self-supervised learning strategy, the rods can adapt to different velocities and accelerations unseen during training and produce plausible simulations.

4.2 Shell Simulation

We now turn to cloth simulation by applying our approach to simulate a discrete elastic shell by incorporating the StVK stretching energy and hinge-based bending energy under the influence of gravity. To generate training and testing motions, we pin two corners of the shell and animate them with varying velocities along a linear trajectory. We train the neural integrator using the first half of the motion sequence (750 frames) and test it on the latter half, as depicted in Fig. 5. The results demonstrate that our neural integrator successfully generates plausible motion that adheres to the boundary conditions and completes the trajectory smoothly.

4.3 Deformable Solid Simulation

In the last sets of experiments (Fig. 6), we demonstrate results on deformable solids discretized by volumetric finite elements. We fix the upper points (as indicated by red spheres) of an upside-down armadillo and move it along a prescribed trajectory with varying velocities. We train on the initial 60% of the sequence (780 frames) and test on the complete sequence (1300 frames). Our approach captures the nonlinear deformation in real time and remains stable even for unseen motions.

We demonstrate another example in Fig. 7 by showcasing a pair of deformable bunny ears (blue) attached to a rigid bunny head (green) with a prescribed motion. We train on the first 60% of the sequence, which consists of 540 frames, and test on the complete sequence, comprising 900 frames. Our method captures the dynamic motion of the ears under gravity and the change in motion of the bunny head, highlighting its effectiveness in handling complex scenarios involving both rigid and deformable objects.

4.4 Comparisons

Comparisons with Offline Simulation. We compare our neural integrator with our reference offline simulation. As can be seen in Table 1, our method improves the performance by 3 orders of magnitude. All timings are reported on CPU.

Comparisons with Latent Space Integrator. While linear subspace simulation methods benefit from a constant map from reduced to full space, they require more bases for the same reconstruction quality [Fulton et al. 2019]. We therefore favor nonlinear subspace simulation methods and compared our method with state-of-the-art methods by Fulton et al. [2019] and Shen et al. [2021]. Both methods

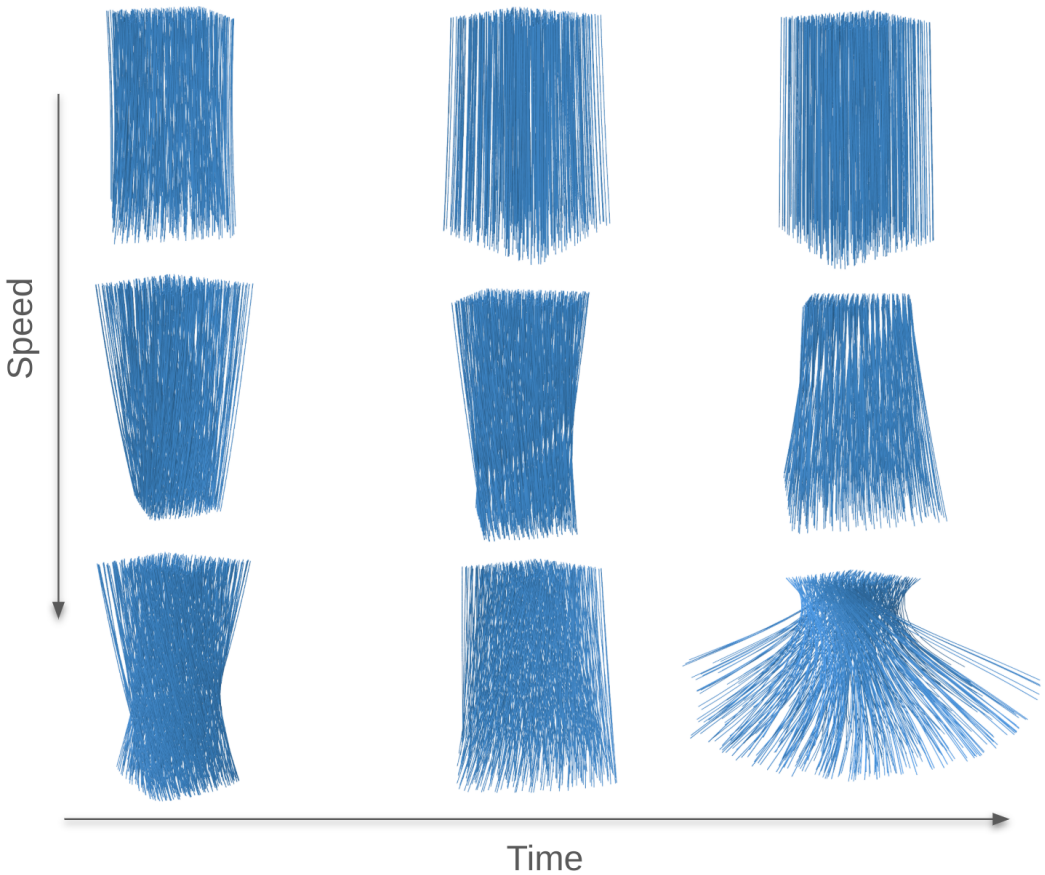


Fig. 4. **Rods Under Rotation Boundary Conditions:** Our method produces plausible dynamics when adapting to changes in different boundary conditions, *i.e.* rods swing much higher at large rotation speeds (third row) but do not accumulate large momentum when the rotation speed is small to medium (first and second row).

leverage autoencoders to construct nonlinear spaces and perform optimization-based integration in the subspace. At inference time, both approaches require full space reconstructions from latent codes. The energies as well as their derivatives for optimization are computed at selected and optimized *cutature* points. On the contrary, our method entirely bypasses these computations by predicting next-step latent codes directly using a neural integrator. In this section, we show that our approach is faster to compute when compared to even a single computation of the energy and derivative required for a single *cutature* point. In our implementation, we do not explicitly construct the Jacobian matrix, but instead rely on a convenient Jacobian-vector product function provided by PyTorch. This timing is reported in the second-to-last column of Table 2.

4.5 Ablation Studies

Comparison with Supervised Learning. We attribute robustness and stability to our self-supervised training strategy. In this example (Fig.8), we compare the rollout stability of our method with that of a supervised strategy. The first and last row use identical network parameters, while the only

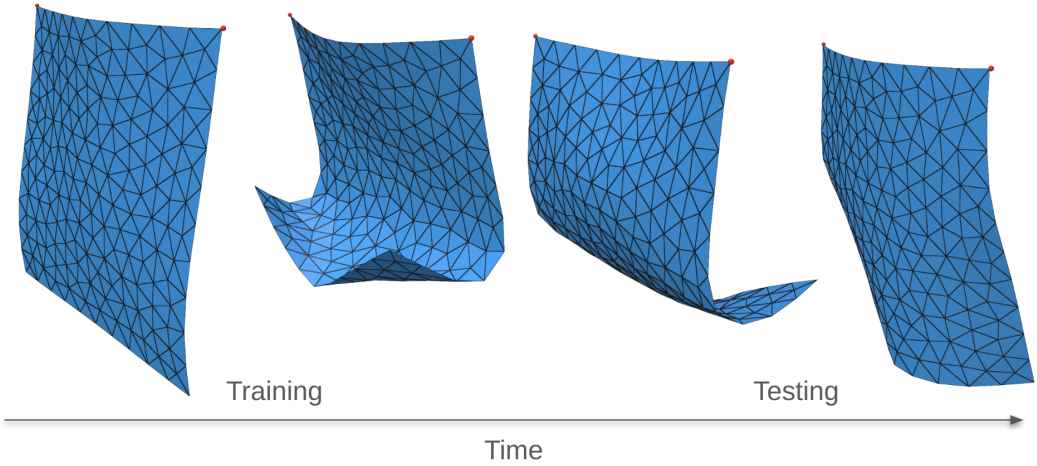


Fig. 5. **Moving Cloth:** Two pinned corners of a piece of cloth are being moved along a linear trajectory. Our method is able to generate stable simulation outcomes for a longer time horizon, despite being trained on only half of the sequence.

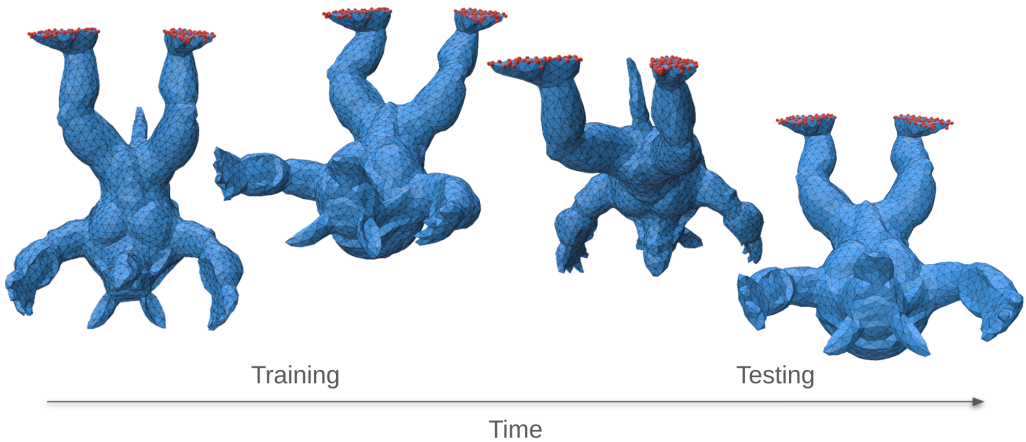


Fig. 6. **Swinging Armadillo:** Our method simulates the elastic deformation of an upside-down armadillo under gravity, with the prescribed motion of the boundary vertices shown in red. The simulation accurately captures the nonlinear behavior of the dynamic motion and demonstrates generalization to unseen poses.

difference is the loss function. In the supervised setting, while the network converges to its local minimum, the L_2 error is still non-zero. During inference, only the first two frames precisely match the training data, and the per-time-step prediction error rapidly deviates from the training data distribution. Consequently, errors accumulate, causing autoregressive inference to diverge in fewer than 100 frames. While the L_2 error can be reduced by increased network capacity (row 2-3), the supervised approach still suffers from stability issues. Our method is robust to rollout errors and remains stable after thousands of steps. For our method, we use an MLP of 5 layers of 256 neurons. For the supervised setting, we include the number of layers and the number of neurons per layer on the left.

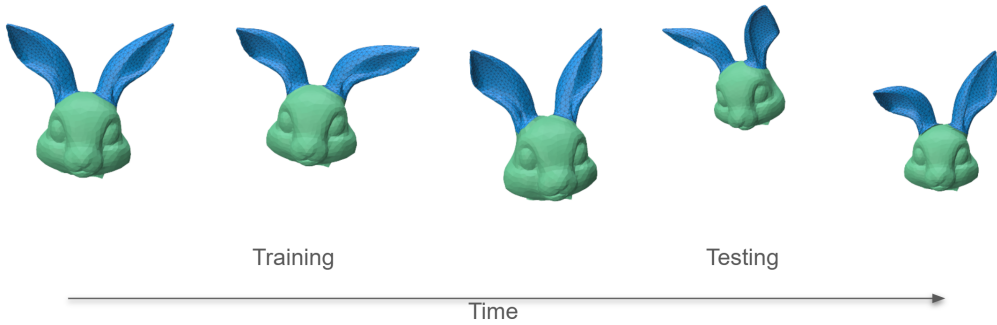


Fig. 7. **Bunny Ears:** We simulate the elastic deformation of a pair of bunny ears attached to a rigid bunny head, with the prescribed motion of the head shown in green. The simulation captures the dynamic movement of the ears under gravity and predicts their motion on unseen sequences.

Table 1. **Quantitative comparison against reference offline simulation.** By improving the performance by orders of magnitudes, our method achieves real-time performance on CPU.

Examples	Full Space DoF	Subspace DoF	Simulation	Ours Integration	Ours Decoder	Ours Total
Hair Rotation	10,800	4	268 ms	0.264 ms	0.456 ms	0.720 ms
Hair Translation	5,400	4	208 ms	0.172 ms	0.386 ms	0.558 ms
Cloth	576	4	18.83 ms	0.109 ms	0.163 ms	0.272 ms
Armadillo	10,020	12	136.8 ms	0.253 ms	0.236 ms	0.489 ms
Bunny Ears	8,046	8	112.6 ms	0.228 ms	0.198 ms	0.426 ms

Data Balancing. While our physics-based loss function automatically accounts for the weighting of different terms, data within each batch can still have energies in different value ranges, *e.g.*, rapidly changing boundary conditions can lead to comparatively large momentum and elastic energies and vice versa. As can be seen in Fig. 9, without data balancing (*row 1*), the rods curl much more inward compared to the ground truth data (*row 3*) whereas our approach reproduces the desired motion (*row 2*).

Training Noise. In this example (Fig. 10), we show that adding noise during training helps prevent overfitting. We simulate a cantilever beam under gravity load with one end being fixed. With first-order implicit Euler integration, the simulation converges to a steady-state solution. We train our network using the first 100 frames of the sequence with and without training noise. During testing, we roll out 200 more frames than the training sequence.

In the second example, we study the effect of our training noise in a more complex setting. Our training data points only contain states that strictly satisfy the boundary conditions and obey the laws of physics. While our self-supervised loss function penalizes the deviations of equilibrium states for the third step, small errors in this prediction can still lead to divergence during autoregressive inference (as can be seen from the first row). By adding noise to the input latents, we effectively sample out-of-balance states during training. Consequently, we achieve stable rollouts that satisfy the boundary conditions at all times (second row).

Table 2. **Quantitative comparison against latent space integrator.** We compare our complete method against the simplest setting in an optimization-based latent space integration framework, *i.e.* computing the Jacobian vector product for a single full space vertex w.r.t. the latent space variables once. In reality, more than one cubature is required, and computing this gradient more than once is necessary. Nonetheless, we show that our complete approach is already faster than this single operation.

Examples	Full Space DoF	Subspace DoF	Decoder Layers	Integrator Layers	Computing Jvp	Ours
Hair Rotation	10,800	4	512, 512, 512, 50	512, 512, 512	2.19 ms	0.720 ms
Hair Translation	5,400	4	256, 256, 256, 50	256, 256, 256	1.51 ms	0.558 ms
Cloth	576	4	200, 200, 200, 50	32, 32	0.564 ms	0.272 ms
Armadillo	10,020	12	200, 200, 200, 50	256, 256, 256, 256, 256	0.649 ms	0.489 ms
Bunny Ears	8,046	8	200, 200, 200, 50	256, 256, 256, 256, 256	0.632 ms	0.426 ms

4.6 Autoencoder Training

Our autoencoder reconstruction achieves a low error with no visible artifacts or visual errors. This high-fidelity reconstruction is crucial as larger errors can introduce spurious forces in full space, which hinders subsequent self-supervised training. The training time of the autoencoder ranges from 5 minutes to 30 minutes, depending on the complexity of the object geometry.

4.7 Timings

All timings in Tables 1 and 2 are reported from a workstation with an Nvidia 3080 GPU and an AMD Threadripper CPU. Our training process consists of 10,000 epochs, with each epoch taking less than 1 second to complete. The total training time is approximately 3 hours.

5 CONCLUSION & FUTURE WORK

We have proposed a novel paradigm for real-time dynamic simulation of elastic objects in latent space. By leveraging a small neural network function exclusively in latent space, we accelerate offline simulation by orders of magnitude. We further proposed training noise and batch-weighted data normalization techniques to ensure stability for long-horizon autoregressive inference and data balancing.

While our method enables real-time simulation at 30 FPS, it currently does not support varying frame rates at test time. Similar to existing subspace simulation methods, the nonlinear subspaces learned by our autoencoders are restricted to a single geometry and topology. Although beyond the scope of this work, applying topology independent model reduction techniques [Modi et al. 2024] could be a promising direction for generalizing across geometries. Our method could be extended to handle contact with a sufficiently smooth representation [Du et al. 2024; Larionov et al. 2021; Li et al. 2020], and further reduction can be explored leveraging neural contact methods [Romero et al. 2023, 2022, 2021]. Additionally, although material parameters could potentially be integrated as trainable variables, our approach does not allow online exploration of deformation behaviors across

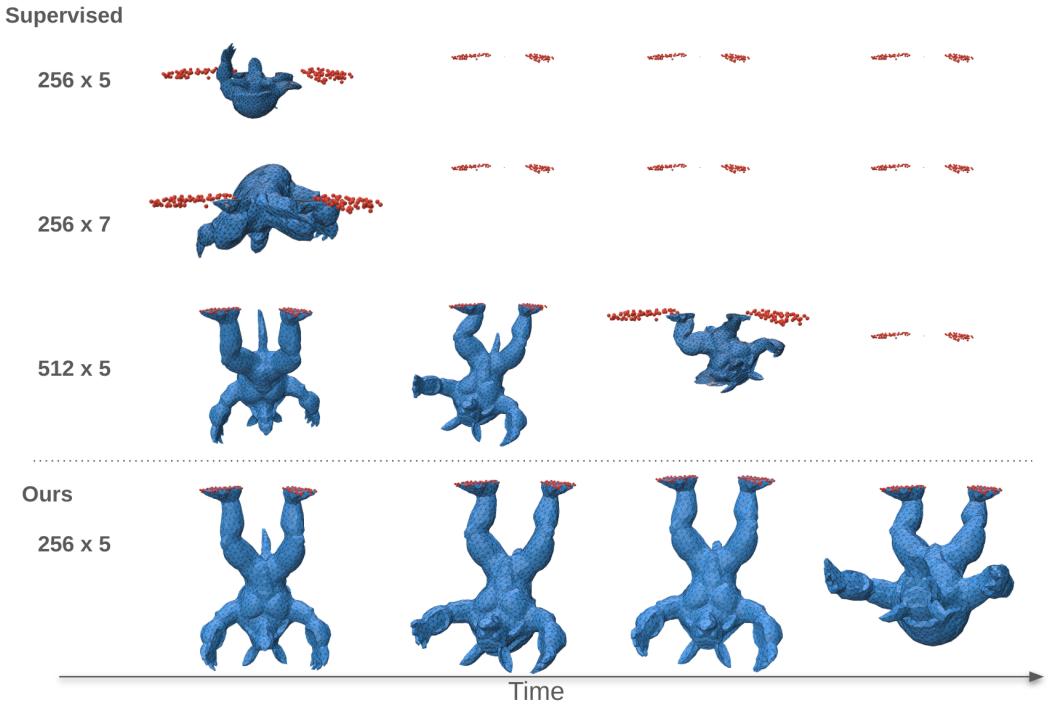


Fig. 8. **Autoregressive Inference:** We compare our approach with a supervised learning strategy. Supervised learning lacks stability when it comes to long rollouts due to per-step error accumulation. While increasing network capacity mitigates this issue to some extent (row 1-3), it diverges eventually for a thousand-frame sequence. On the contrary, our method (row 4) enables stable simulation roll outs with plausible dynamics.

different materials. We have demonstrated that our method is more robust and stable compared to supervised alternatives; however, the kinetic energy in our simulated results remains lower than that observed in ground-truth simulation data (see Fig. 12). Our method currently works with simulation data only; extending the same paradigm to captured data, or reconstructed data given by point cloud or Gaussian splats, is another exciting direction for future exploration.

ACKNOWLEDGMENTS

We thank Ryan Goldade for his assistance with the experiments and Wenzhao Xu for her help with the figures. We further thank the anonymous reviewers for their valuable feedback and suggestions.

REFERENCES

- Jernej Barbič, Marco da Silva, and Jovan Popović. 2009. Deformable object animation using reduced optimal control. In *ACM SIGGRAPH 2009 papers*. 1–9.
- Jernej Barbič and Doug L James. 2005. Real-time subspace integration for St. Venant-Kirchhoff deformable models. *ACM transactions on graphics (TOG)* 24, 3 (2005), 982–990.
- Jernej Barbič, Funshing Sin, and Eitan Grinspun. 2012. Interactive editing of deformable simulations. *ACM Transactions on Graphics (TOG)* 31, 4 (2012), 1–8.
- Otman Benckroun, Jiayi Eris Zhang, Siddhartha Chaudhuri, Eitan Grinspun, Yi Zhou, and Alec Jacobson. 2023. Fast Complementary Dynamics via Skinning Eigenmodes. *ACM Transactions on Graphics (TOG)* 42, 4 (2023), 1–21.
- Miklós Bergou, Basile Audoly, Etienne Vouga, Max Wardetzky, and Eitan Grinspun. 2010. Discrete viscous threads. *ACM Transactions on graphics (TOG)* 29, 4 (2010), 1–10.

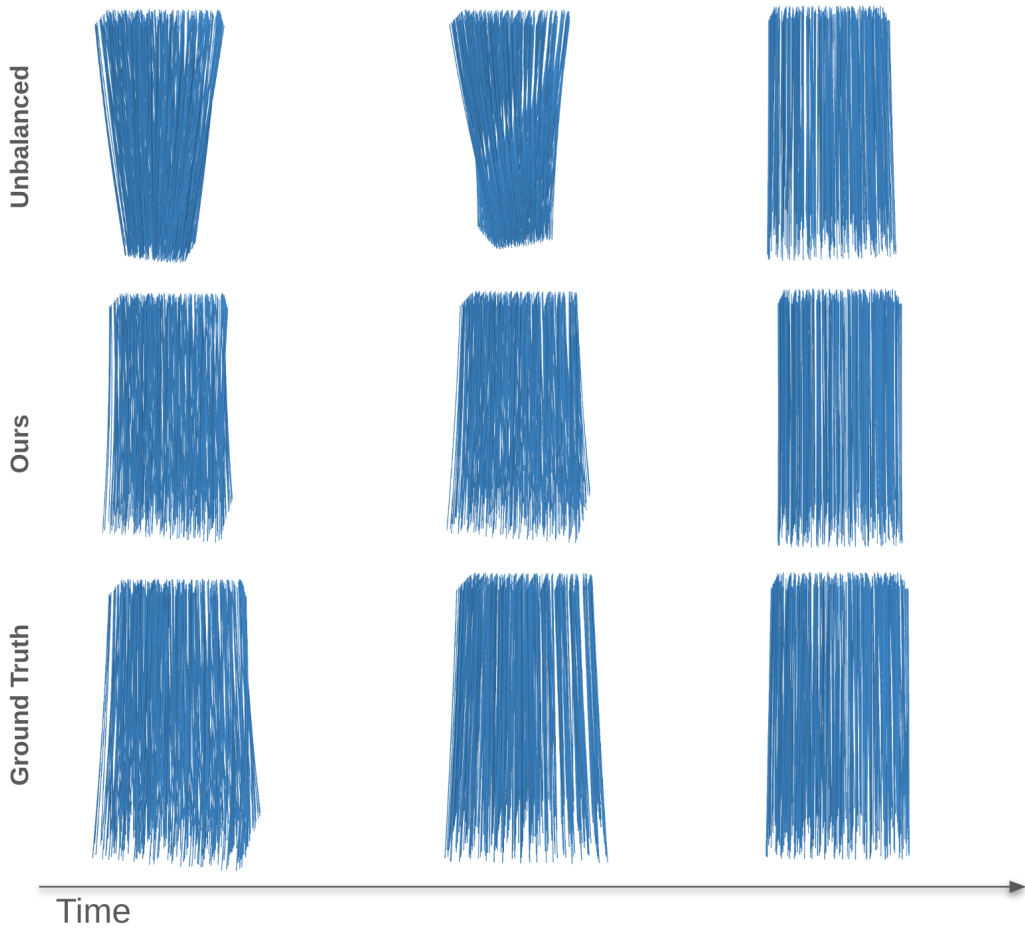


Fig. 9. **Data Balancing:** Without balancing data between different system energies, the training process tends to favor high energy states due to the correspondingly large gradients. Using our balanced loss function improves the prediction, especially on low energy states.

- Miklós Bergou, Max Wardetzky, Stephen Robinson, Basile Audoly, and Eitan Grinspun. 2008. Discrete elastic rods. In *ACM SIGGRAPH 2008 papers*. 1–12.
- Hugo Bertiche, Meysam Madadi, and Sergio Escalera. 2020. Pbnns: Physically based neural simulator for unsupervised garment pose space deformation. *arXiv preprint arXiv:2012.11310* (2020).
- Hugo Bertiche, Meysam Madadi, and Sergio Escalera. 2022. Neural cloth simulation. *ACM Transactions on Graphics (TOG)* 41, 6 (2022), 1–14.
- Gaurav Bhokare, Eisen Montalvo, Elie Diaz, and Cem Yuksel. 2024. Real-Time Hair Rendering with Hair Meshes. In *ACM SIGGRAPH 2024 Conference Papers*. 1–10.
- Menglei Chai, Changxi Zheng, and Kun Zhou. 2014. A reduced model for interactive hairs. *ACM Transactions on Graphics (TOG)* 33, 4 (2014), 1–11.
- Yue Chang, Peter Yichen Chen, Zhecheng Wang, Maurizio M Chiaramonte, Kevin Carlberg, and Eitan Grinspun. 2023. LiCROM: Linear-Subspace Continuous Reduced Order Modeling with Neural Fields. In *SIGGRAPH Asia 2023 Conference Papers*. 1–12.
- Peter Yichen Chen, Maurizio M Chiaramonte, Eitan Grinspun, and Kevin Carlberg. 2023. Model reduction for the material point method via an implicit neural representation of the deformation map. *J. Comput. Phys.* 478 (2023), 111908.

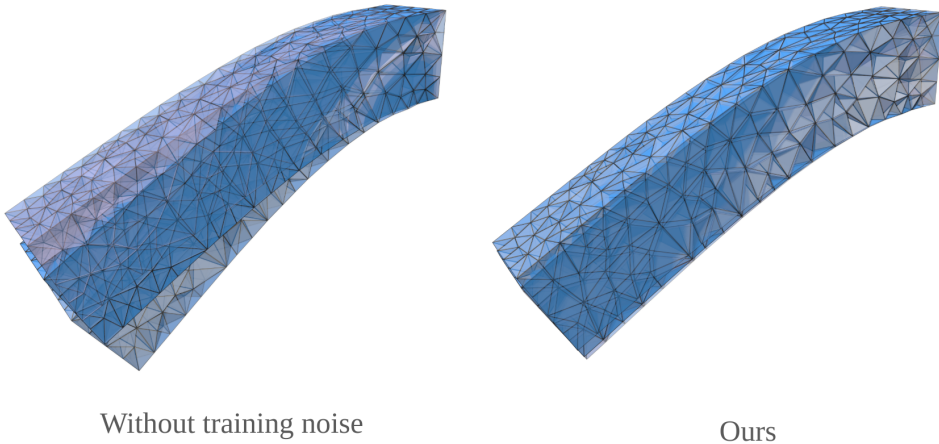


Fig. 10. **Steady State Solution:** A cantilever beam clamped from one end is deformed under gravity. After training on the initial 100 frames of the simulation sequence, we continue the inference of the network for an additional 200 frames. The last frames of the inference are shown with decreasing transparency. Without training noise, the network prediction oscillates around the steady state solution (*left*), whereas the training noise facilitates the network converging to the ground truth solution (*right*).

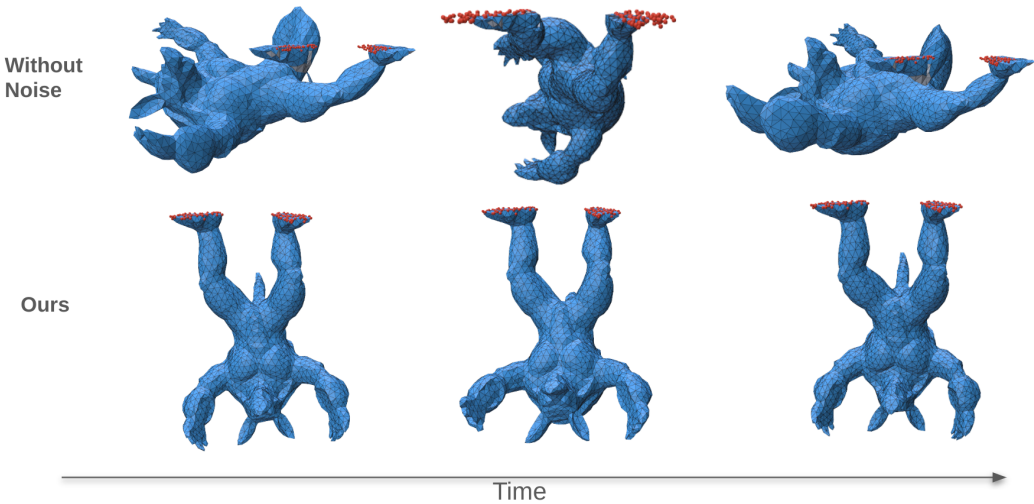


Fig. 11. **Training Noise:** Without training noise, the network predictions gradually deviate from the boundary conditions and generate implausible states containing significantly large deformations. With training noise, our network predictions satisfy boundary conditions at all times.

Peter Yichen Chen, Jinxu Xiang, Dong Heon Cho, Yue Chang, GA Pershing, Henrique Teles Maia, Maurizio M Chiamonte, Kevin Carlberg, and Eitan Grinspun. 2022. Crom: Continuous reduced-order modeling of pdes using implicit neural representations. *arXiv preprint arXiv:2206.02607* (2022).

Nuttapong Chentanez, Miles Macklin, Matthias Müller, Stefan Jeschke, and Tae-Yong Kim. 2020. Cloth and skin deformation with a triangle mesh based convolutional neural network. In *Computer Graphics Forum*, Vol. 39. Wiley Online Library, 123–134.

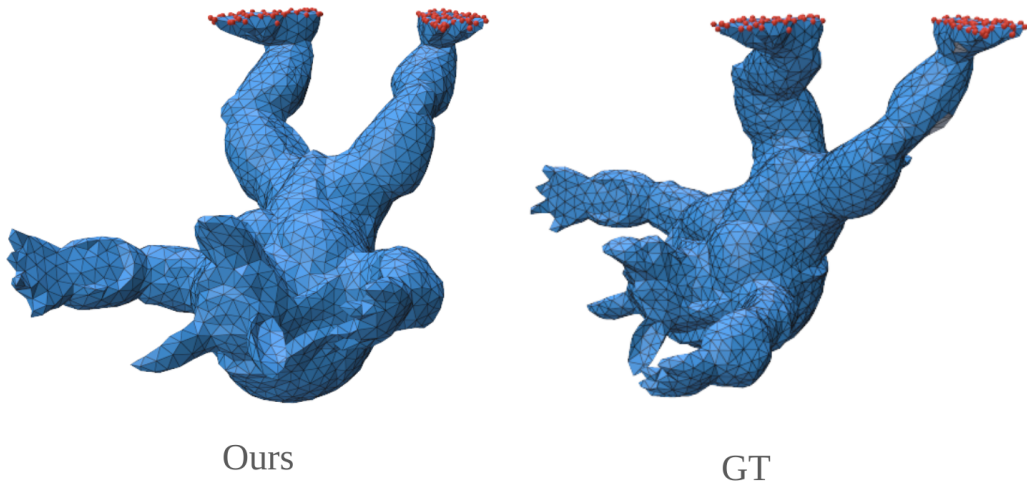


Fig. 12. **Limitation:** our prediction (left), albeit stable, exhibits kinetic energy loss compared to the ground truth data (right).

- Edilson De Aguiar, Leonid Sigal, Adrien Treuille, and Jessica K Hodgins. 2010. Stable spaces for real-time clothing. *ACM Transactions on Graphics (ToG)* 29, 4 (2010), 1–9.
- Yinwei Du, Yue Li, Stelian Coros, and Bernhard Thomaszewski. 2024. Robust and Artefact-Free Deformable Contact with Smooth Surface Representations. In *Computer Graphics Forum*. Wiley Online Library, e15187.
- Simon Duenser, Bernhard Thomaszewski, Roi Poranne, and Stelian Coros. 2022. Nonlinear compliant modes for large-deformation analysis of flexible structures. *ACM Transactions on Graphics* 42, 2 (2022), 1–11.
- Lawson Fulton, Vismay Modi, David Duvenaud, David IW Levin, and Alec Jacobson. 2019. Latent-space dynamics for reduced deformable simulation. In *Computer graphics forum*, Vol. 38. Wiley Online Library, 379–391.
- Artur Grigorev, Giorgio Becherini, Michael Black, Otmar Hilliges, and Bernhard Thomaszewski. 2024. Contourcraft: Learning to resolve intersections in neural multi-garment simulations. In *ACM SIGGRAPH 2024 Conference Papers*. 1–10.
- Artur Grigorev, Bernhard Thomaszewski, Michael J Black, and Otmar Hilliges. 2023. Hood: Hierarchical graphs for generalized modelling of clothing dynamics. In *Proceedings of the IEEE/CVF Conference on Computer Vision and Pattern Recognition*. 16965–16974.
- Eitan Grinspun, Anil N Hirani, Mathieu Desbrun, and Peter Schröder. 2003. Discrete shells. In *Proceedings of the 2003 ACM SIGGRAPH/Eurographics symposium on Computer animation*. Citeseer, 62–67.
- Fabian Hahn, Bernhard Thomaszewski, Stelian Coros, Robert W Sumner, Forrester Cole, Mark Meyer, Tony DeRose, and Markus Gross. 2014. Subspace clothing simulation using adaptive bases. *ACM Transactions on Graphics (TOG)* 33, 4 (2014), 1–9.
- Oshri Halimi, Tuur Stuyck, Donglai Xiang, Timur M Bagautdinov, He Wen, Ron Kimmel, Takaaki Shiratori, Chenglei Wu, Yaser Sheikh, and Fabian Prada. 2022. Pattern-Based Cloth Registration and Sparse-View Animation. *ACM Trans. Graph.* 41, 6 (2022), 196–1.
- David Harmon and Denis Zorin. 2013. Subspace integration with local deformations. *ACM Transactions on Graphics (TOG)* 32, 4 (2013), 1–10.
- Kris K Hauser, Chen Shen, and James F O’Brien. 2003. Interactive Deformation Using Modal Analysis with Constraints. In *Graphics Interface*. Citeseer, 247.
- Kaiming He, Xiangyu Zhang, Shaoqing Ren, and Jian Sun. 2016. Deep residual learning for image recognition. In *Proceedings of the IEEE conference on computer vision and pattern recognition*. 770–778.
- Daniel Holden, Bang Chi Duong, Sayantan Datta, and Derek Nowrouzezahrai. 2019. Subspace neural physics: Fast data-driven interactive simulation. In *Proceedings of the 18th annual ACM SIGGRAPH/Eurographics Symposium on Computer Animation*. 1–12.
- Jerry Hsu, Tongtong Wang, Zherong Pan, Xifeng Gao, Cem Yuksel, and Kui Wu. 2024. Real-time Physically Guided Hair Interpolation. *ACM Transactions on Graphics (TOG)* 43, 4 (2024), 1–11.
- Sagar Imambi, Kolla Bhanu Prakash, and GR Kanagachidambaresan. 2021. PyTorch. *Programming with TensorFlow: solution for edge computing applications* (2021), 87–104.

- Alec Jacobson, Ilya Baran, Ladislav Kavan, Jovan Popović, and Olga Sorkine. 2012. Fast automatic skinning transformations. *ACM Transactions on Graphics (ToG)* 31, 4 (2012), 1–10.
- Theodore Kim and John Delaney. 2013. Subspace fluid re-simulation. *ACM Transactions on Graphics (TOG)* 32, 4 (2013), 1–9.
- Egor Larionov, Ye Fan, and Dinesh K. Pai. 2021. Frictional Contact on Smooth Elastic Solids. *ACM Trans. Graph.* 40, 2, Article 15 (April 2021), 17 pages. <https://doi.org/10.1145/3446663>
- Kookjin Lee and Kevin T Carlberg. 2020. Model reduction of dynamical systems on nonlinear manifolds using deep convolutional autoencoders. *J. Comput. Phys.* 404 (2020), 108973.
- Minchen Li, Zachary Ferguson, Teseo Schneider, Timothy R Langlois, Denis Zorin, Daniele Panozzo, Chenfanfu Jiang, and Danny M Kaufman. 2020. Incremental potential contact: intersection-and inversion-free, large-deformation dynamics. *ACM Trans. Graph.* 39, 4 (2020), 49.
- Xuan Li, Yu Fang, Lei Lan, Huamin Wang, Yin Yang, Minchen Li, and Chenfanfu Jiang. 2023. Subspace-preconditioned gpu projective dynamics with contact for cloth simulation. In *SIGGRAPH Asia 2023 Conference Papers*. 1–12.
- Yue Li et al. 2024. WuKong. (2024). <https://github.com/liyuesolo/Wukong2024>.
- Yue Li, Marc Habermann, Bernhard Thomaszewski, Stelian Coros, Thabo Beeler, and Christian Theobalt. 2021. Deep physics-aware inference of cloth deformation for monocular human performance capture. In *2021 International Conference on 3D Vision (3DV)*. IEEE, 373–384.
- Aoran Lyu, Shixian Zhao, Chuhua Xian, Zhihao Cen, Hongmin Cai, and Guoxin Fang. 2024. Accelerate Neural Subspace-Based Reduced-Order Solver of Deformable Simulation by Lipschitz Optimization. *ACM Transactions on Graphics (TOG)* 43, 6 (2024), 1–10.
- Qing Lyu, Menglei Chai, Xiang Chen, and Kun Zhou. 2020. Real-time hair simulation with neural interpolation. *IEEE Transactions on Visualization and Computer Graphics* 28, 4 (2020), 1894–1905.
- Pingchuan Ma, Peter Yichen Chen, Bolei Deng, Joshua B Tenenbaum, Tao Du, Chuang Gan, and Wojciech Matusik. 2023. Learning neural constitutive laws from motion observations for generalizable pde dynamics. In *International Conference on Machine Learning*. PMLR, 23279–23300.
- Sebastian Martin, Bernhard Thomaszewski, Eitan Grinspun, and Markus Gross. 2011. Example-based elastic materials. In *ACM SIGGRAPH 2011 papers*. 1–8.
- Vismay Modi, Nicholas Sharp, Or Perel, Shinjiro Sueda, and David IW Levin. 2024. Simplicits: Mesh-Free, Geometry-Agnostic Elastic Simulation. *ACM Transactions on Graphics (TOG)* 43, 4 (2024), 1–11.
- Jorge Nocedal and Stephen J Wright. 1999. *Numerical optimization*. Springer.
- Shaowu Pan, Steven L Brunton, and J Nathan Kutz. 2023. Neural implicit flow: a mesh-agnostic dimensionality reduction paradigm of spatio-temporal data. *Journal of Machine Learning Research* 24, 41 (2023), 1–60.
- Alex Pentland and John Williams. 1989. Good vibrations: Modal dynamics for graphics and animation. In *Proceedings of the 16th annual conference on Computer graphics and interactive techniques*. 215–222.
- Tobias Pfaff, Meire Fortunato, Alvaro Sanchez-Gonzalez, and Peter Battaglia. 2020. Learning Mesh-Based Simulation with Graph Networks. In *International Conference on Learning Representations*.
- Cristian Romero, Dan Casas, Maurizio Chiamonte, and Miguel A Otaduy. 2023. Learning Contact Deformations with General Collider Descriptors. In *SIGGRAPH Asia 2023 Conference Papers*. 1–10.
- Cristian Romero, Dan Casas, Maurizio M Chiamonte, and Miguel A Otaduy. 2022. Contact-centric deformation learning. *ACM Transactions on Graphics (TOG)* 41, 4 (2022), 1–11.
- Cristian Romero, Dan Casas, Jesús Pérez, and Miguel Otaduy. 2021. Learning contact corrections for handle-based subspace dynamics. *ACM Transactions on Graphics (TOG)* 40, 4 (2021), 1–12.
- Alvaro Sanchez-Gonzalez, Jonathan Godwin, Tobias Pfaff, Rex Ying, Jure Leskovec, and Peter Battaglia. 2020. Learning to simulate complex physics with graph networks. In *International conference on machine learning*. PMLR, 8459–8468.
- Igor Santesteban, Miguel A Otaduy, and Dan Casas. 2022. Snug: Self-supervised neural dynamic garments. In *Proceedings of the IEEE/CVF Conference on Computer Vision and Pattern Recognition*. 8140–8150.
- Nicholas Sharp, Cristian Romero, Alec Jacobson, Etienne Vouga, Paul Kry, David IW Levin, and Justin Solomon. 2023. Data-Free Learning of Reduced-Order Kinematics. In *ACM SIGGRAPH 2023 Conference Proceedings*. 1–9.
- Siyuan Shen, Yin Yang, Tianjia Shao, He Wang, Chenfanfu Jiang, Lei Lan, and Kun Zhou. 2021. High-order differentiable autoencoder for nonlinear model reduction. *ACM Transactions on Graphics* 40, 4 (2021).
- Eftychios Sifakis and Jernej Barbic. 2012a. FEM simulation of 3D deformable solids: a practitioner’s guide to theory, discretization and model reduction. In *ACM SIGGRAPH 2012 Courses (SIGGRAPH ’12)*. Association for Computing Machinery, New York, NY, USA, Article 20, 50 pages. <https://doi.org/10.1145/2343483.2343501>
- Eftychios Sifakis and Jernej Barbic. 2012b. FEM simulation of 3D deformable solids: a practitioner’s guide to theory, discretization and model reduction. In *Acm siggraph 2012 courses*. 1–50.
- Tuur Stuyck, Gene Wei-Chin Lin, Egor Larionov, Hsiao-yu Chen, Aljaz Bozic, Nikolaos Sarafianos, and Doug Roble. 2025. Quaffure: Real-Time Quasi-Static Neural Hair Simulation. In *Proceedings of the Computer Vision and Pattern Recognition Conference*. 239–249.

- Joseph Teran, Eftychios Sifakis, Geoffrey Irving, and Ronald Fedkiw. 2005. Robust quasistatic finite elements and flesh simulation. In *Proceedings of the 2005 ACM SIGGRAPH/Eurographics symposium on Computer animation*. 181–190.
- Adrien Treuille, Andrew Lewis, and Zoran Popović. 2006. Model reduction for real-time fluids. *ACM Transactions on Graphics (TOG)* 25, 3 (2006), 826–834.
- Jiahong Wang, Yinwei Du, Stelian Coros, and Bernhard Thomaszewski. 2024. Neural Modes: Self-supervised Learning of Nonlinear Modal Subspaces. In *Proceedings of the IEEE/CVF Conference on Computer Vision and Pattern Recognition*. 23158–23167.
- Yu Wang, Alec Jacobson, Jernej Barbič, and Ladislav Kavan. 2015. Linear subspace design for real-time shape deformation. *ACM Transactions on Graphics (TOG)* 34, 4 (2015), 1–11.
- Kui Wu and Cem Yuksel. 2016. Real-time hair mesh simulation. In *Proceedings of the 20th ACM SIGGRAPH Symposium on Interactive 3D Graphics and Games*. 59–64.
- Xiaofeng Wu, Rajaditya Mukherjee, and Huamin Wang. 2015. A unified approach for subspace simulation of deformable bodies in multiple domains. *ACM Transactions on Graphics (TOG)* 34, 6 (2015), 1–9.
- Cem Yuksel, Scott Schaefer, and John Keyser. 2009. Hair meshes. *ACM Transactions on Graphics (TOG)* 28, 5 (2009), 1–7.
- Jonas Zehnder, Yue Li, Stelian Coros, and Bernhard Thomaszewski. 2021. Ntopo: Mesh-free topology optimization using implicit neural representations. *Advances in Neural Information Processing Systems* 34 (2021), 10368–10381.
- Meng Zhang, Tuanfeng Y. Wang, Duygu Ceylan, and Niloy J. Mitra. 2021. Dynamic neural garments. *ACM Trans. Graph.* 40, 6, Article 235 (Dec. 2021), 15 pages. <https://doi.org/10.1145/3478513.3480497>
- Mianlun Zheng and Jernej Barbic. 2024. Multi-Resolution Real-Time Deep Pose-Space Deformation. *ACM Transactions on Graphics (TOG)* 43, 6 (2024), 1–11.
- Zhongtian Zheng, Tongtong Wang, Qijia Feng, Zherong Pan, Xifeng Gao, and Kui Wu. 2024. Proxy Asset Generation for Cloth Simulation in Games. *ACM Transactions on Graphics (TOG)* 43, 4 (2024), 1–12.
- Zeshun Zong, Xuan Li, Minchen Li, Maurizio M Chiamonte, Wojciech Matusik, Eitan Grinspun, Kevin Carlberg, Chenfanfu Jiang, and Peter Yichen Chen. 2023. Neural stress fields for reduced-order elastoplasticity and fracture. In *SIGGRAPH Asia 2023 Conference Papers*. 1–11.